LOCALIZING SOURCES OF HORIZONTAL ORBIT OSCILLATIONS AT RHIC*

R. Calaga, R. Michnoff, T. Satogata
BNL, NY 11973, USA

Abstract

Horizontal oscillations of the closed orbit at frequencies around 10Hz are observed at RHIC. These oscillations lead to beam beam offsets at the collision point, resulting in emittance growth and reduced luminosity. An approach to localize the sources of these vibrations using a special mode of RHIC turn-by-turn BPM data is presented. Data from the 2005-6 are analyzed to spatially resolve the location of the dominant sources.

INTRODUCTION

Closed orbit oscillations at frequencies close to 10 Hz (7800 turn periodicity) are observed in RHIC during regular operation which reach several millimeters in the focusing triplets ($\beta^* \sim 1$ m). This gives rise to modulated beam-beam jitter at the interaction point (IP) which can lead to emittance growth and luminosity loss for sufficiently large beam-beam offsets. The existing beam position monitor (BPM) system offers the following acquisition modes:

- Averaged orbit of 10^4 turns which can be acquired only every 4 seconds. In this mode the 10 Hz oscillation is averaged over 1.25 periods and therefore not easily observed.
- Turn-by-turn mode but the buffer only has limited memory to acquire 1024 turns which is not sufficient to observe the oscillation with acceptable phase resolution.
- There are eight BPMs (two per ring per plane) equipped with a large buffer to acquire up to to a million turns ($\sim$ 10 sec of data) which is sufficient to sample the 10 Hz signal. However, only two BPMs per plane are insufficient to use for localization of the source. Also the size of the data is quite large which is impractical to implement on hundreds of BPMs around the ring.

SPECIAL ACQUISITION MODE

A modification in the low-level software of the BPM acquisition system overcame the data buffer limit by acquiring only every nth turn instead of every consecutive turn. An appropriate selection of n allows analysis at the frequency under study ($n \propto f_{rev}/f$). The revolution frequency at RHIC is 78 KHz. Acquisition of one orbit every 78 turns ($n = 78$) for 1024 orbits provides approximately one second of data. Therefore, analysis of orbit oscillations at 10 Hz becomes feasible. Data from the 2006 proton-proton run using this BPM system configuration are shown in Fig. 1. The y axis shows the 1-sigma deviation of the orbit amplitude acquired for a one second period. The oscillation amplitude is significantly smaller in the vertical plane indicating that the source of the jitter is mainly horizontal.

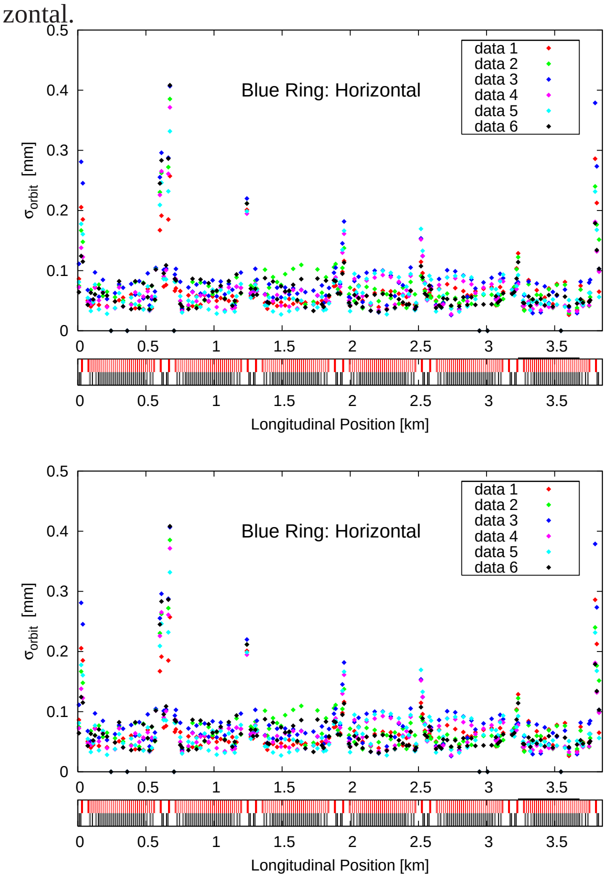

Figure 1: Top: 1σ deviation of 1024 orbits each acquired from single turn sampled at 1 kHz is plotted as a function of longitudinal position for the Blue ring.

The orbit in the focusing triplets reaches several millimeters and can pose aperture constraints for smaller β^* in addition to the beam-beam related emittance growth and luminosity loss. Until such jitter is damped it may be impossible to operate at betatron tunes close to the integer required for better beam-beam performance [1]. Fig. 2 shows the 1 kHz sampled orbits at two BPMs located in IR6 and IR8 for 1024 acquisitions.

* This work was performed under the auspices of the US Department of Energy

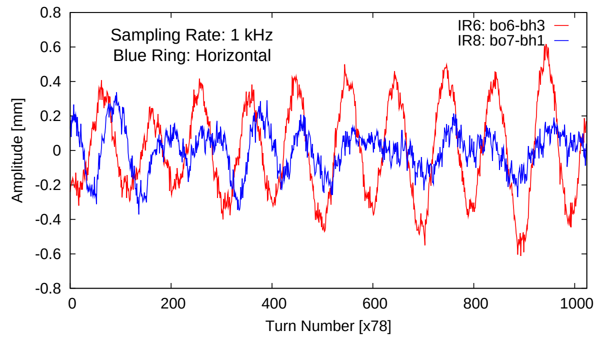

Figure 2: The closed orbit oscillations in the horizontal and vertical plane as recorded in the IR BPMs in the Blue ring as a function of turn number (sampled at 1 kHz).

SVD ANALYSIS

Any matrix $X_{n\times m}$ can be factorized into the form

$$X = U\Sigma V^{\dagger} \tag{1}$$

The number of non-zero diagonal elements of Σ (singular values) reveal the dimensionality of the data set. The vectors $\{u_1, u_2, \ldots, u_n\}$ in U and $\{v_1, v_2, \ldots, v_m\}$ in V represent the and temporal and spatial signatures of the dominant modes that describe the dynamics of the system under study. Fig. 3 shows the singular value spectrum of the matrix consisting of the 1024 acquired orbits at all BPMs at a sampling rate of 1 kHz. The spectrum depicts a few dominant modes well above the noise floor. The spectrum also consists of a long tail mainly dominated by noise since BPMs in a single turn acquisition mode have a poor signal to noise ratio.

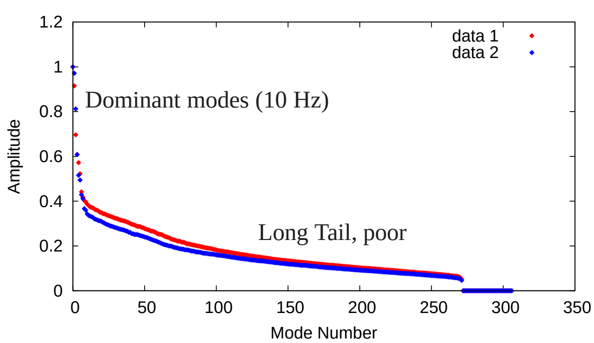

Figure 3: The singular value spectrum of 1024 orbits acquired at 1 kHz sampling rate at all BPMs around the ring.

The frequency spectrum of the temporal vectors of the first few dominant modes as shown in Fig. 4 clearly attribute these modes to the 10Hz orbit oscillations. The data matrix contains orbit acquisitions from both the horizontal and vertical plane arranged consecutively. The spatial vectors of the dominant modes only exhibit signal in the first half of the vector indicating that the orbit vibrations are mainly in the horizontal plane. Although, the spatial vector is distributed around the ring in the horizontal plane, distinct spikes appear in each of the three modes pointing to possible location for the jitter source. Mechanical and beam-based analysis performed in Ref. [2] report that these vibrations coincide with mechanical vibration modes of the cold masses due to the liquid helium flow.

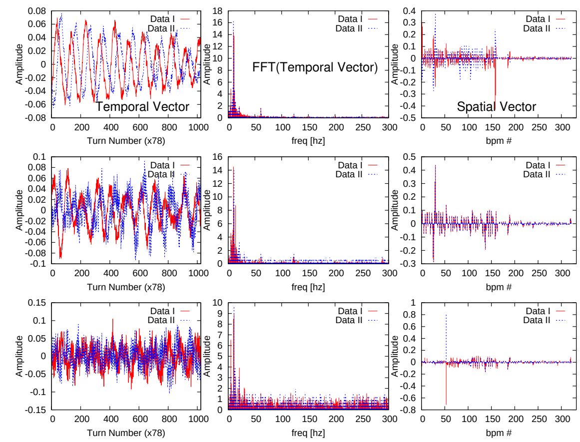

Figure 4: Left/right: Temporal and spatial vectors of the first three dominant modes of the orbit matrix acquired at a sampling rate of 1 kHz. Middle: The frequency spectrum of the corresponding temporal modes.

CORRECTION

Based on the information from the SVD modes a closed orbit correction was employed to localize the sources of the jitter from difference orbits of the acquired data. The difference orbits between acquisitions separated by approximately half a period were used to attain maximum amplitude of the signal. In addition successive difference orbits ($\pm$) up to some predetermined number with respect to the orbit were used accumulate statistics. For example, if D is the data matrix constructed from 1024 orbits such as,

$$D = \begin{pmatrix} t_1 & \ddots & & \\ - & - & - & - \\ \vdots & \ddots & & \\ t_{50} & & & \\ \vdots & & & \\ - & - & - & - \\ \vdots & & & \\ t_{1024} & & & \ddots \end{pmatrix}$$

A difference orbit d_j orbit vector is given by

$$\vec{d_j} = \vec{t}_{j+(50\pm40)} - \vec{t_j} \tag{2}$$

where j is the successive orbit acquisitions at 1 kHz sampling rate.

The difference orbits at all BPMs were used as measurement vector to perform a least squares type orbit correction using the available dipole correctors in RHIC.

$$(\vec{\theta}_i^x, \vec{\theta}_i^y)^T = A^{-1}(\vec{\delta x}_i, \vec{\delta y}_i)^T \tag{3}$$

$$A_{mn} = \frac{\sqrt{\beta_m\beta_n}}{2\sin(\pi\nu_x)} \cos(|\phi_m - \phi_n| - \pi\nu_x) \tag{4}$$

where, A_{mn} is the linear response matrix of n^{th} corrector which yields an associated orbit at m BPMs [3]. Typically the system is over-determined since $m > n$, therefore the solution minimizes the quadratic residual, $\|A\vec{\theta} - \vec{d}\|^2$. Fig. 5 shows a sample correction vector θ_i^x for a horizontal orbit correction from two different difference orbits. Orbit correctors near IR10 region appear as best correctors to minimize the orbit jitter. Orbit correctors at the other IRs are also used but the strengths are a factor 3-6 smaller. It should be noted that the $\beta^* = 5$ m at IP10 compared to IP6 and IP8 which have $\beta^* = 1$ m. Therefore, the beta functions in the triplet quadrupoles in the IR10 are considerably smaller than those found in the triplets of IR6 and IR8. A possible source of the oscillation other than the focusing triplets as proposed in Ref. [2] could be the abort kickers in the IR10 region [4], but further investigation is required. Correctors with the largest strengths in Fig. 5 are on the right side of IR10 in the proximity of the abort kicker.

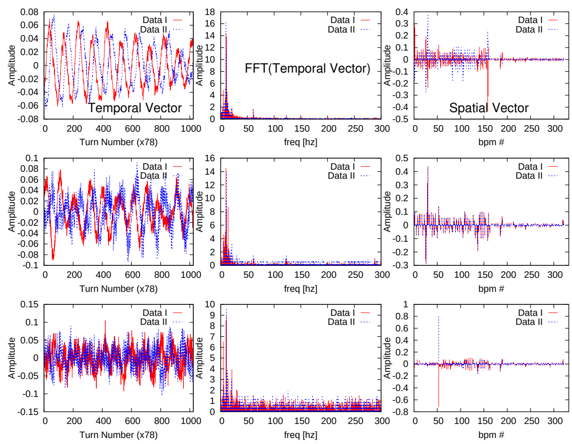

Figure 5: Sample correction of two difference orbits from the acquired data. Correctors near IR10 are appear to correct the RMS orbit by a factor of 3 or better in the Blue ring for both samples.

The correction vector was computed for several difference orbits (d_j) and for several data sets (D) and were accumulated into a histogram weighted by their corresponding corrector strengths. It is evident from Fig. 7 that the correctors in IR10 are two orders of magnitude larger than the rest of the IRs. This confirms the IR10 solution to be independent of the choice of the difference orbit (j) used for the correction, and the choice of the data set D.

To confirm the effectiveness of the correction, the RMS orbit before and the simulated orbit after correction were accumulated into a histogram for the same cases as in Fig. 6. The simulated RMS orbit for both the Yellow and Blue rings are reduced by a factor of 3 or better in all cases as shown in Fig. 7. A real correction would entail dynamic correction vector (feedback) at 10 Hz or similar. Although, the source of the jitter is not yet identified from this analysis, a fast orbit feedback system using a few correctors in the IR10 region may be sufficient to significantly suppress the oscillations.

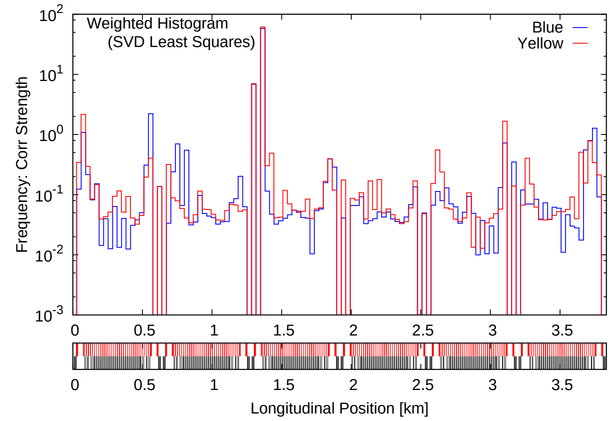

Figure 6: Top: Histogram of orbit correctors weighted by their strength to correct the difference orbits obtained from the 1 kHz acquisitions accumulated over several difference orbits (d_j) and data sets (D).

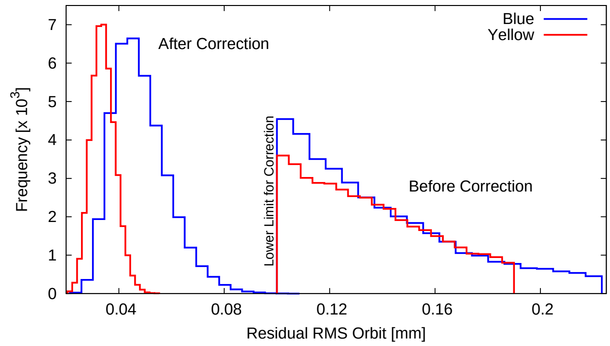

Figure 7: Histogram of the residual rms orbit before and after correction in both the rings.

CONCLUSIONS

A modification of the BPM low level software enabled the acquisition of orbits at every n^{th} turn and observations of the orbit oscillations at low frequencies with the existing BPM system. SVD analysis and a least squares type orbit correction on the difference orbits indicate that a few correctors in IR10 region suppress the oscillation by a factor of 3 or better. Statistics of correction over a large set of difference orbits confirms this observation. Analysis of data sets acquired in run 2007-08 is underway to track the evolution of the best correctors.

ACKNOWLEDGMENTS

he authors would like to thank W. Fischer, C. Montag, T. Roser, and R. Tomas for useful discussions.

REFERENCES

[1] C. Montag et al., EPAC08, Genova, 2008.

[2] C. Montag et al., NIMA, Vol 564, Issue 1, 1 August 2006.

[3] A. Chao et al., Handbook of accelerator physics and Engineering, 1998 (sec. 4.5.3).

[4] T. Roser, Private communication.